Temperature-dependent formation and evolution of the interfacial dislocation network of Ag/Pt(111)

Maciej Jankowski, Herbert Wormeester, Harold J. W. Zandvliet, and Bene Poelsema
Physics of Interfaces and Nanomaterials, MESA+ Institute for Nanotechnology, University of Twente, P.O. Box 217, 7500AE Enschede, the Netherlands

(Received 20 March 2014; revised manuscript received 19 May 2014; published 3 June 2014)

We have investigated the formation of a dislocation network that develops at the interface of a Ag film on Pt(111) and its evolution with film thickness at 600 K and above. This system is commonly considered to be representative of a surface-confined alloy, and we have studied the structure and topography of the films' surfaces up to thicknesses of 35 ML using high-resolution low-energy electron diffraction. The network is formed during the growth of the second layer and is fully developed already for films only a few layers thick. The spacing of the network varies between 5.8 and 6.6 nm when grown at 600 and 800 K, respectively. This dependence on the growth temperature is attributed to a temperature-dependent material mixing in the first (few) layers of the film. This mixing is irreversibly set by the deposition temperature and even persists during prolonged annealing at a temperature close to the desorption of Ag from Pt(111).

DOI: 10.1103/PhysRevB.89.235402 PACS number(s): 68.35.Fx, 68.49.Jk, 81.10.Pq

I. INTRODUCTION

The heteroepitaxial growth of an ultrathin film results in strain formation, which can be relieved via the formation of well-ordered, periodic patterns [1,2]. The possibility to tune the chemical and physical properties of such structures offers a wide variety of applications ranging from growth of self-assembled nanostructures [3–5] to creating desired catalytic properties of such structures [6]. The patterns of these well-ordered nanotemplates are the result of self-organization and depend on the intrinsic physical properties of the substrate-adsorbate system. Self-organization provides a viable alternative to lithography-like processes, especially if a typical dimension of just a few tens of atoms is desired. The periodicity of such structures can be controlled with subnanometer accuracy using various parameters, such as chemical composition, growth temperature, and the thickness of the film [7].

A Ag film deposited on a Pt(111) surface [Ag/Pt(111)] is a good example of a self-organized system, which can be used as a nanotemplate. The Ag film is subject to isotropic compressive stress due to the +4.12% lattice mismatch with the underlying platinum substrate at room temperature. At temperatures below about 500 K the first layer of silver grows pseudomorphically on Pt(111). Upon heating, the film becomes disordered [8] and forms a surface-confined alloy [9]. At growth temperatures above 500 K the completion of the first layer is accompanied with a gradual dealloying. During the growth of the second monolayer the stress is relieved by the formation of a triangular dislocation network [10]. This dislocation network in the second monolayer was interpreted in terms of fcp and hcp stacking regions, separated by repulsively interacting dislocation lines. Recent experiments showed that this model does not suffice [11,12]. In the revised description, partial dislocations are created in the first monolayer at fcc-stacking sites, and both the first and the second monolayers contain intermixed regions of Pt and Ag atoms. The third layer was found to be almost perfectly hexagonal and contains exclusively Ag atoms without stacking faults. However, the buried defects in the first monolayer cause a spatial undulation of the subsequent layers. Such a height undulation as a result of a dislocation network is very similar to observations of the Ge/Si(111) system as reported by Horn-von Hoegen *et al.* [13] using high-resolution electron diffraction. This technique enables a detailed view of the average periodicity of the dislocation network, which is still lacking for the frequently studied Ag/Pt(111) system.

In this paper, we report on the investigation of the Ag/Pt(111) system and show how undulated Ag layers with a specific periodicity and symmetry of the buried dislocation network evolve at various growth temperatures and film thicknesses. We concentrate on film thicknesses above 3 monolayers (ML), a regime that has been hardly illuminated so far. The growth of thicker films leads to an attenuation of the surface undulation and thus a smoother surface. We also focus on the order of both the distance between dislocation lines and the effects of intermixing in the first few layers in relation to the lateral variation of the composition.

II. EXPERIMENT

The experiments were conducted in an ultrahigh vacuum chamber with a base pressure of 1×10^{-10} mbar. Diffraction patterns were recorded with two complementary low-energy electron diffraction (LEED) systems, a high-resolution Omicron Spot Profile Analysis LEED (SPA-LEED) and an OCI Vacuum Engineering multichannel plate LEED (MCP-LEED). While the first system combines a high lateral resolution with a high dynamic range for intensity measurements, the latter allows us to record images at a video rate with a much lower electron beam current density and recording of I-V spectra. The system was further equipped with a residual gas analyzer (Stanford Research RGA-200) and Auger electron spectroscopy (AES).

The sample temperature of the Pt(111) crystal was monitored with a K-type thermocouple. The thermocouple wires were spot welded directly to the crystal with a dedicated YAG laser, which resulted in a small and very stable welding contact. Surface cleaning was done by prolonged repetitive cycles of argon ion bombardment, annealing at 800 K in oxygen at 2×10^{-7} mbar, and subsequent flashing to 1300 K. This resulted in a surface with a contamination level below the

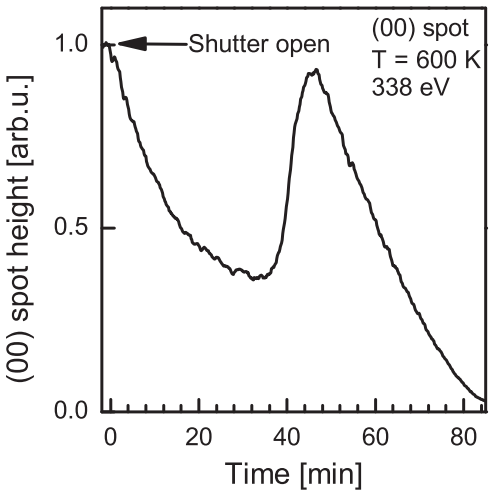

FIG. 1. The normalized height of the (00) spot during deposition of silver at 600 K. The data were taken with 338-eV electrons.

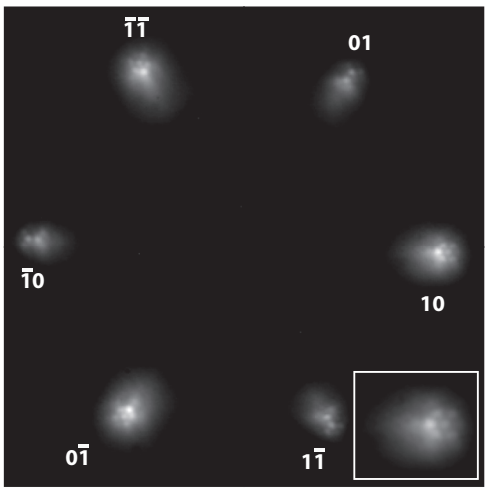

FIG. 2. A 144-eV MCP-LEED pattern after deposition of 5-ML silver on Pt(111) at 800 K. The inset is an enlargement of the (10) spot. The electron gun blocks the view of the (00) spot.

sensitivity of AES and a surface that exhibits a sharp LEED pattern. The full width at half maximum (FWHM) of the (00) spot was about 0.3% of the Brillouin zone (BZ). Corrected for the instrument function, this reflects an average surface terrace width of about 94 nm.

Silver was deposited with an Omicron EFM-3 evaporator from a molybdenum crucible. The evaporator was mounted at an angle of 55° with respect to the SPA-LEED sample axis. For *in situ* monitoring of the (00) LEED spot during deposition, the SPA-LEED was retracted and positioned at a distance of 56 mm between the sample and the front plate of SPA-LEED. All diffraction patterns presented in this work were recorded after deposition of silver at an elevated temperature (i.e., 600 or 800 K), followed by cooling down to 100 K.

The silver deposition rate was calibrated by tracking the evolution of the (00) spot height, measured at an energy of 338 eV during the deposition of Ag on a Pt(111) surface at 600 K. An example is shown in Fig. 1. Similar to the height characteristics obtained in thermal energy atom scattering (TEAS) experiments [8], we can observe an initial decay of the (00) spot height caused by the formation of silver clusters embedded in the platinum layer at a coverage <0.5 ML and platinum clusters embedded in the silver layer at higher coverages [14]. The increase of the height of the (00) spot after 35 min indicates an increase of the order due to coalescence and growth of the islands during the completion of the first, pseudomorphic silver layer. The maximum intensity after 47 min is assumed to correspond to the completion of the monolayer [15] and is used to calibrate the Ag evaporation rate.

III. RESULTS AND DISCUSSION

A. Mechanism of satellite spot formation

Figure 2 shows an electron diffraction pattern of a 5-ML Ag film deposited on a Pt(111) surface at 800 K. The first-order diffraction spots of the clean Pt(111) surface are surrounded by satellite spots, as shown in the inset in Fig. 2. This feature was also observed with thermal energy helium atom scattering [16]. As thermal energy helium atoms are not very sensitive to in-plane or subsurface features, we conclude that these features can be attributed to height undulations. Such a set of satellite peaks was also observed for several other systems, among which are Fe/W(110), Ge/Si(111), Bi(111)/Si(001), Ag(111)/Si(111), Co/Pd(111), etc. [17–21]. The lattice mismatch between the film and the substrate induces stress in the first few layers of the film for these material combinations. This stress is relieved through the creation of well-ordered dislocation arrays with features related to symmetry, stacking, and periodicity, which depend on the lattice mismatch, film thickness, deposition temperature, and substrate orientation. Beyond the first monolayer, the dislocations at the film-substrate interface cause a periodic height undulation, which persists up to the topmost layer and decreases with increasing film thickness.

At first glance, the Ag/Pt(111) is very similar to the Ge/Si(111) system. The lattice mismatch in both cases is +4.2%, and both show a triangular dislocation network which exhibits a similar evolution of the network symmetry with increasing coverage. Therefore, the analysis of the LEED spectra developed for the Ge/Si(111) system by Horn von Hoegen *et al.* [22] will be used to describe the Ag/Pt(111) system.

B. Formation of the dislocation network at low coverage

In Fig. 3 we present two series of diffraction features centered around the ($\bar{1}$0) spot for film thicknesses as indicated, recorded at 600 K [shown in Fig. 3(a)] and 800 K [shown in Fig. 3(b)]. At 1 ML we observe a single diffraction spot at both temperatures, whose position in the BZ corresponds to the lattice constant of the clean Pt(111) surface. The fact that we do not observe any additional features in the diffraction patterns, including those taken at different electron energies indicates that the film is pseudomorphic at 1 ML. As we increase the coverage further to 1.2 ML, very weak and rather diffuse satellite spots emerge around the integer-order spots at a distance that relates to the lattice mismatch of the two materials. The intensity of these spots increases with coverage, although they

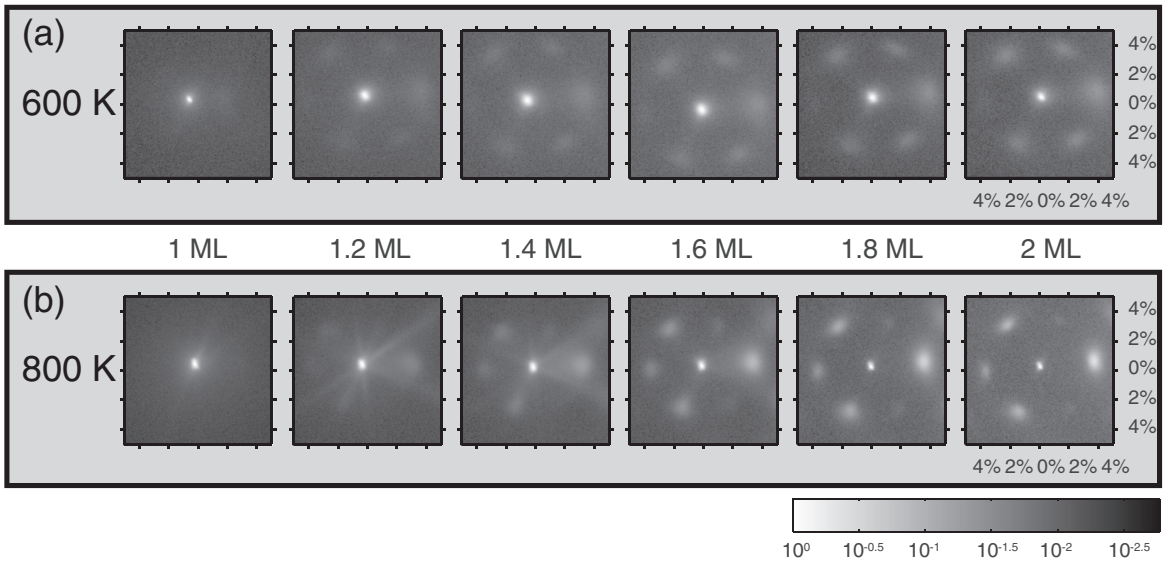

FIG. 3. Series of the $(\bar{1}0)$ spot and its environment after deposition of several amounts of silver, expressed in monolayers, on Pt(111) at (a) 600 K and (b) 800 K. The intensity of the spots is normalized and presented on a logarithmic scale. The energy of the electron beam is 334 and 342 eV at 600 and 800 K, respectively. The x and y axes are expressed as percentage of the BZ calibrated to a clean Pt(111). The origin does not coincide with the absolute $(\bar{1}0)$ spot position for clean Pt(111).

are still very weak and substantially broader compared to the clean Pt Bragg spot. This limits the precision with which the separation between the spots can be determined. An approximate value of this distance is 3.4%–3.8% of the BZ. This implies a periodicity of the dislocation network of 6.3–7.0 nm.

The satellite spots indicate the presence of a periodic height undulation on the surface. From this we conclude that the formation of the dislocation network coincides with the formation of the second monolayer. This confirms the current model that states that during the deposition of this second layer the compressive strain in the first monolayer is released through realloying of the Ag with Pt and stacking faults [11]. An optimal recording of the satellite spots at a deposition temperature of 600 and 800 K was obtained at slightly different energies, 334 eV in Fig. 3(a) and 342 eV in Fig. 3(b), respectively. Figure 3(b) also shows very weak lines crossing the main spot at 800 K for a coverage between 1.2 and 1.6 ML. From these two observations, we conclude that the two series of spots recorded at 600 and 800 K originate from a different dislocation network. This is in agreement with scanning tunneling microscopy (STM) measurements carried out at 600 and 800 K, where hexagonal and triangular networks were observed, respectively [23].

C. Dislocation networks at 600 and 800 K: Smoothening of the surface

The evolution of the surface height undulation beyond 2-ML film thickness is displayed in Fig. 4. At 2 ML, the most intense spot corresponds to the first-order diffraction from the Pt(111) surface. This spot is significantly attenuated for a 5-ML-thick film [see Fig. 4(b)]. At the same time, the spot at the central position in Fig. 4(b), which is separated from the Pt(111) spot by about 4% of the BZ, gains intensity at the expense of the Pt$(\bar{1}0)$ spot. The position of this central spot corresponds to the lateral lattice parameter of the Ag film. The intensity of the surrounding satellite spots has significantly increased, and even third-order satellite spots are observed. A series of linear profiles through the Pt$(\bar{1}0)$ and the Ag$(\bar{1}0)$ spots recorded at different coverages is shown in Fig. 5.

With a further increase of film thickness the intensity of the satellites spots compared to the Ag(111) spot decreases, and the spots are no longer distinguishable for films thicker than 20 ML [see Fig. 4(i)]. Since the elastic mean free path of 334-eV electrons is only about 4 layers (i.e., only 2 back and forth), direct contributions from the interface can safely be ignored beyond film thicknesses of 8 layers. We relate the gradual decline of the satellite spots to the continuous smoothening of the surface, i.e., through an attenuation of the height undulation. This is a natural consequence of the increasing distance between the exposed surface and the dislocations residing at the buried interface. However, the presence of weak satellite spots indicates that the formation of an undulation-free Ag(111) surface on Pt requires a much higher coverage. We observe similar trends for the network formed at 800 K, where even at 36 ML the satellite spots are still visible.

D. Dislocation networks at 600 and 800 K: Relaxation

The $(\bar{1}0)$ spot clearly shows a shift in peak intensity from the Pt Bragg peak to that of the Ag film. The symmetry of the network can be better observed near the specular spot, as shown in Figs. 6 and 7, which show diffraction patterns around the (00) spot, recorded for various coverages at 600 and 800 K, respectively. For a comparison of the surface morphology we have used a number of distinct coverages and an electron energy of 334 eV for both temperatures. Like the $(\bar{1}0)$ spot recorded at 600 K (see Fig. 4), the intensity of the satellite spots surrounding the specular beam is attenuated with increasing coverage for both temperatures. However, very weak satellite spots are still visible up to coverages as high as 26 and 35 ML at 600 and 800 K, respectively.

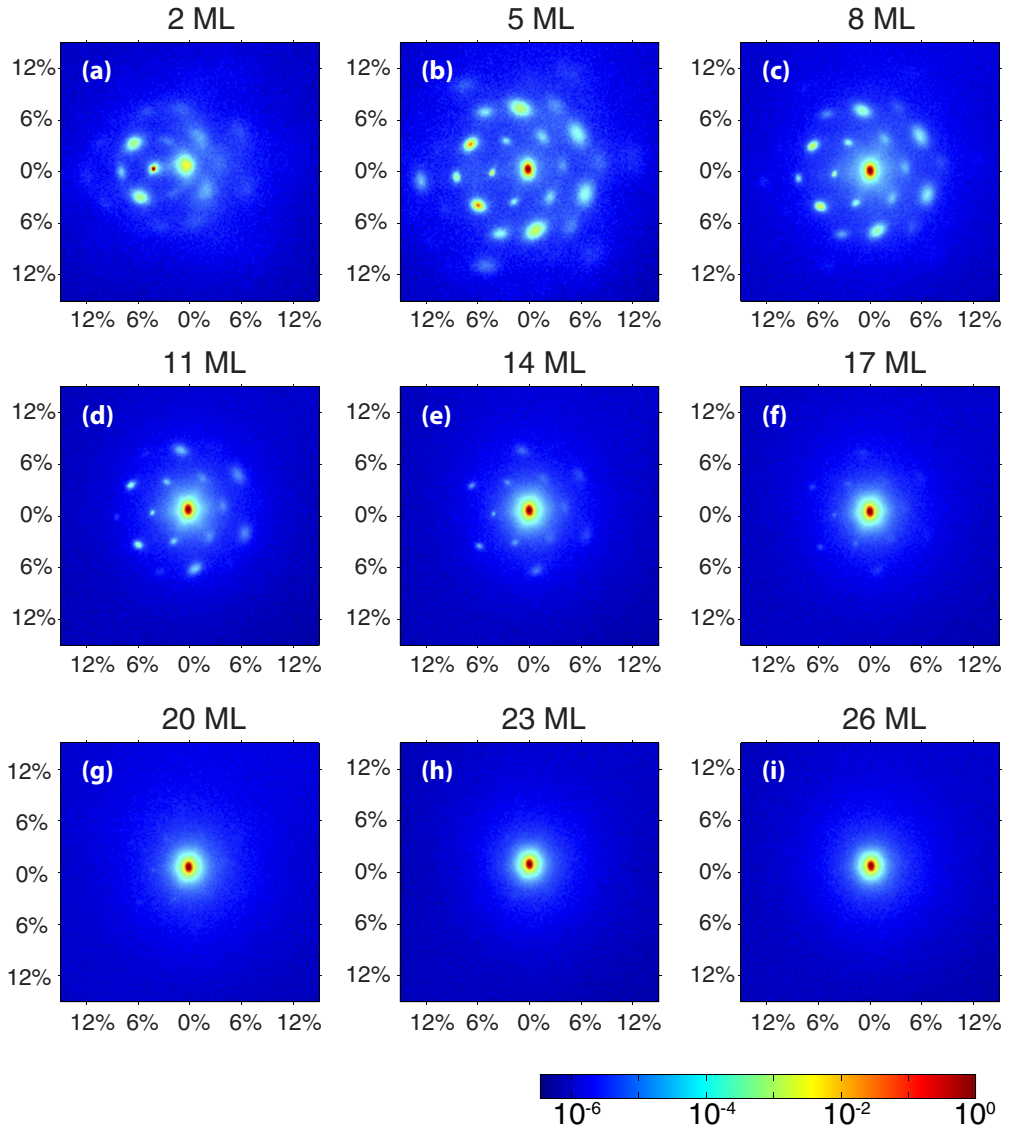

FIG. 4. (Color online) Series of $(\bar{1}0)$ spot patterns after deposition of silver on Pt(111) at 600 K. The intensity of the spots is normalized with respect to the maximum value and presented on a logarithmic scale. The energy of the electron is 334 eV. The x and y axes are expressed as the percentage of the BZ calibrated to a clean Pt(111). The origin does not coincide with the absolute $(\bar{1}0)$ spot position for clean Pt(111).

An important parameter that describes the dislocation network is the distance between dislocation lines, which can be extracted from the separation of the satellite spots in the diffraction pattern. Figure 8 shows a plot of this separation between the satellite spots in units of the BZ vs Ag coverage at temperatures of 600 and 800 K. At 2-ML coverage, the separation of the satellite spots is 3.76% and 3.58% of the BZ at 600 and 800 K, respectively, which increases to 4.15% and 3.65%, respectively, for a 5-ML film (5.9 and 6.5 nm in real space). For films thicker than 5 ML we observe only a slight decrease of the separation between the satellite spots. This trend indicates that the dislocation network relaxes in the first few monolayers. For the fully relaxed bulk lattice, the value of the lattice mismatch at 100 K is 4.00%. It is remarkable that this value is approached closely for the 600 K data in view of the different thermal expansion coefficients of Pt and Ag. The 800 K data show a slightly smaller distance between the satellite spots. The latter is attributed to a remaining and persistent minor mixing of Ag and Pt at the interface that strongly influences the geometry, i.e., the spacing of the dislocation network.

Figure 9 shows the variation of the (00) spot height recorded during deposition of Ag at 800 K. It can clearly be seen that the recorded curve has a different shape than the one recorded at 600 K in Fig. 1. This is attributed to the higher level of intermixing of the Ag and Pt at 800 K, which drives the formation of the dislocation network during the growth of the second monolayer. The different symmetries in the diffraction patterns observed at 600 and 800 K are thus attributed to different levels of intermixing of Ag and Pt in the first two layers. This is consistent with the similar conclusion reached by Schuster *et al.* [24], who showed with STM that the degree of the Ag and Pt intermixing varies strongly in the temperature range from 550 to 900 K. They reported that this influences the morphology of the surface.

We emphasize that the dislocation network appears to be fully developed after deposition of only a few monolayers at a

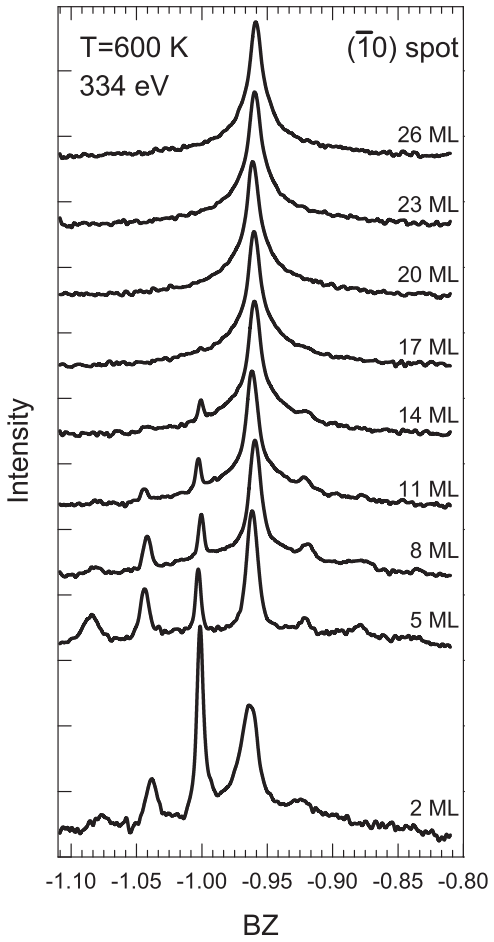

FIG. 5. Series of linear profiles through the $(\bar{1}0)$ spot in the $\langle 10\rangle$ direction for silver deposited at 600 K. The height of the spots is normalized with respect to the Ag(111) spot and is presented on a logarithmic scale. The x axis of the plot is calibrated to the BZ of Pt(111).

given growth temperature. This is further supported by Fig. 10, which shows the diffraction pattern around the specular beam after deposition of 14 ML of Ag at 600 K, followed by a prolonged heating at 800 K, which is below the desorption temperature (∼900 K) of films thicker than 1 ML [25–27]. The obtained pattern continues to bear the characteristic length scale and symmetry of the as-grown 600 K film. This clearly demonstrates that the length scale of the dislocation network is set already in the first few layers and is not affected by prolonged annealing at a 200 K higher temperature.

E. Symmetry of the network

The two series of (00) spot patterns, presented in Figs. 6 and 7, demonstrate a different symmetry of the networks from the relative intensities of the satellite spots. In an attempt to interpret these differences we seek guidance from, in particular, Fig. 11 of Ref. [22]. In that paper the authors describe results obtained for the Ge/Si(111) system, which is distinctly similar to the current Ag/Pt(111) system. In short, any conclusion about the symmetry of the patterns requires caution. For thick layers, with a small amplitude of the undulation, only weak first-order Fourier components are left, leading to a hexagonal shape of the satellite pattern. Indeed, hexagonal structures in the diffuse background are observed at high coverage, both at 600 and 800 K in Figs. 6 and 7. Firm conclusions on the symmetry of the satellite pattern can only be drawn by considering also the intensities of second- and higher-order satellite peaks. Accordingly, we cautiously conclude from Fig. 6 that the films grown at 600 K show hexagonal symmetry. Figure 11 of Ref. [22] also shows that threefold symmetry remains visible if the second-order satellite peaks still carry substantial intensity. On this basis we conclude from the satellite pattern displayed in our Fig. 7 that thinner films grown at 800 K clearly show threefold symmetry. It seems that in the thickness range of 23–29 ML the films transform from threefold into sixfold symmetry. Note that in these cases the second-order satellites still carry sufficient intensity to support this conclusion.

The observed symmetry of the diffraction patterns agrees with the two types of height undulation networks at 2 ML observed previously with scanning tunneling microscopy [23]. For the Ge/Si system these diffraction patterns were explained with a dislocation network [22] as sketched in Fig. 12. Two sets of domain walls for this dislocation network are rotated with respect to each other by 120°. The third set is also rotated by 120° but with some offset with respect to the crossing point of the other two domains. For a nonzero offset, the domain walls do not cross at this same point, and the network is composed of triangular and rhombic areas. In this situation the dislocation network has a threefold symmetry, as shown in Fig. 12(a). However, when the offset is zero, the three domain walls cross at one point, which results in a sixfold-symmetry network [Fig. 12(b)], and the diffraction pattern will also show a sixfold symmetry. A detailed description of this network model can be found in [22].

The observed diffraction patterns for thicker Ag layers on Pt(111) are rationalized as a the gradual evolution of undulations of the surface, initiated by a dislocation network in the second layer, which continues to reside at the interface. The third and consecutive layers cover this network, which causes undulations in the three directions of the higher layers. Although the appearance in reciprocal space is similar to the one observed on Ge/Si, the evolution is different. As for the explanation for the Ge/Si case, the three undulations can either match to give a sixfold symmetry or have an offset leading to the observation of a threefold pattern (see Fig. 12). The undulations are the result of strain fields connected to the buried dislocations. These strain fields interact repulsively, which causes a natural tendency to favor a better ordered hexagonal symmetry for thicker films on Pt(111). We consider this to be the driving force for the gradual change from threefold to sixfold symmetry in the thicker films grown at 800 K.

F. (Dis)order in the network

A closer inspection of the line profiles in Fig. 11 suggests that the FWHM of the satellite peaks depends on their order. The FWHM appears to increase with increasing distance of the satellites from the specular beam. A similar observation is made for the satellites surrounding the $(\bar{1}0)$ order peak, as illustrated by the line profiles in Fig. 5. The same feature

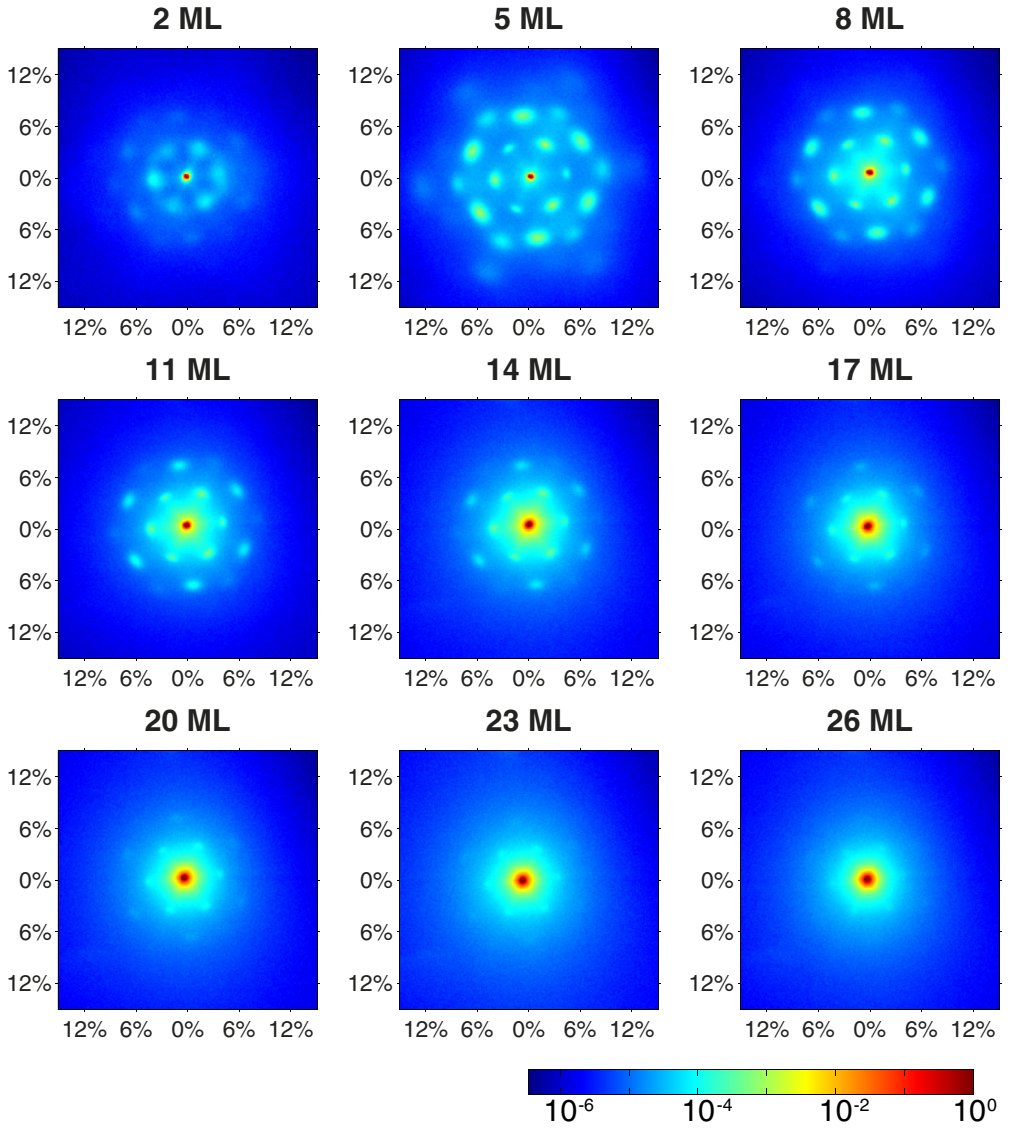

FIG. 6. (Color online) Series of (00) spot patterns after deposition of silver films, with different thicknesses as indicated, on Pt(111) at 600 K. The intensity of the spots is normalized with respect to the height of the specular spot and is presented on a logarithmic scale. The energy of the electrons is 334 eV. The x and y axes of the diffraction patterns are expressed as the percentage of BZ calibrated to a clean Pt(111).

was reported for Ge/Si(111) and was discussed in great detail in Ref. [28]. Horn-von-Hoegen and Henzler demonstrated that this broadening is caused by disorder in the dislocation network. For a simple Markov-type distribution of the distance between the dislocation lines they showed that the FWHM of the satellites should depend on the distance from the host integer peak in a parabolic fashion. Figure 13(a) shows our results for an 8-layer-thick film grown at 800 K and an 8-layer-thick film grown at 600 K. Note that the specular beam is included in the data set since the broadening due to instrumental factors and those due to effects of perpendicular wave vector changes are identical to a very good degree. The 800 K data show a very convincing parabolic relationship between the FWHM of the satellites as a function of the corresponding $\Delta k_{\parallel}$:

$$\mathrm{FWHM} = A + B\Delta k_{\parallel}^{2}. \quad (1)$$

From the fit parameters obtained for the 800 K film we obtain $A = 0.0035$ and $B = 1.36$. The B parameter leads to a standard deviation of 9.4 u.c., with u.c. being the unit cell of the Pt surface. The corresponding mean value of the distance between dislocation lines equals 27.5 u.c. (see Fig. 8). These values are again very similar to those obtained for Ge/Si(111) [28]. The 600 K results are $A = 0.0075$ and $B = 2.45$. For the film grown at 600 K we thus obtain (see Fig. 8) a mean distance of 24.5 u.c. and a standard deviation of 16.8 u.c. The disorder in the 600 K film is substantially higher than that of the 800 K film. The width of the specular beam is, except for the terrace width distribution of the substrate and instrumental factors, determined by the corrugation of the surface. This hints at a higher amplitude of the undulations at 600 K.

In agreement with Ref. [28] we find a reduction of the width of the first-order satellite peaks surrounding the specular spot with increasing film thickness, as shown in Fig. 13(b).

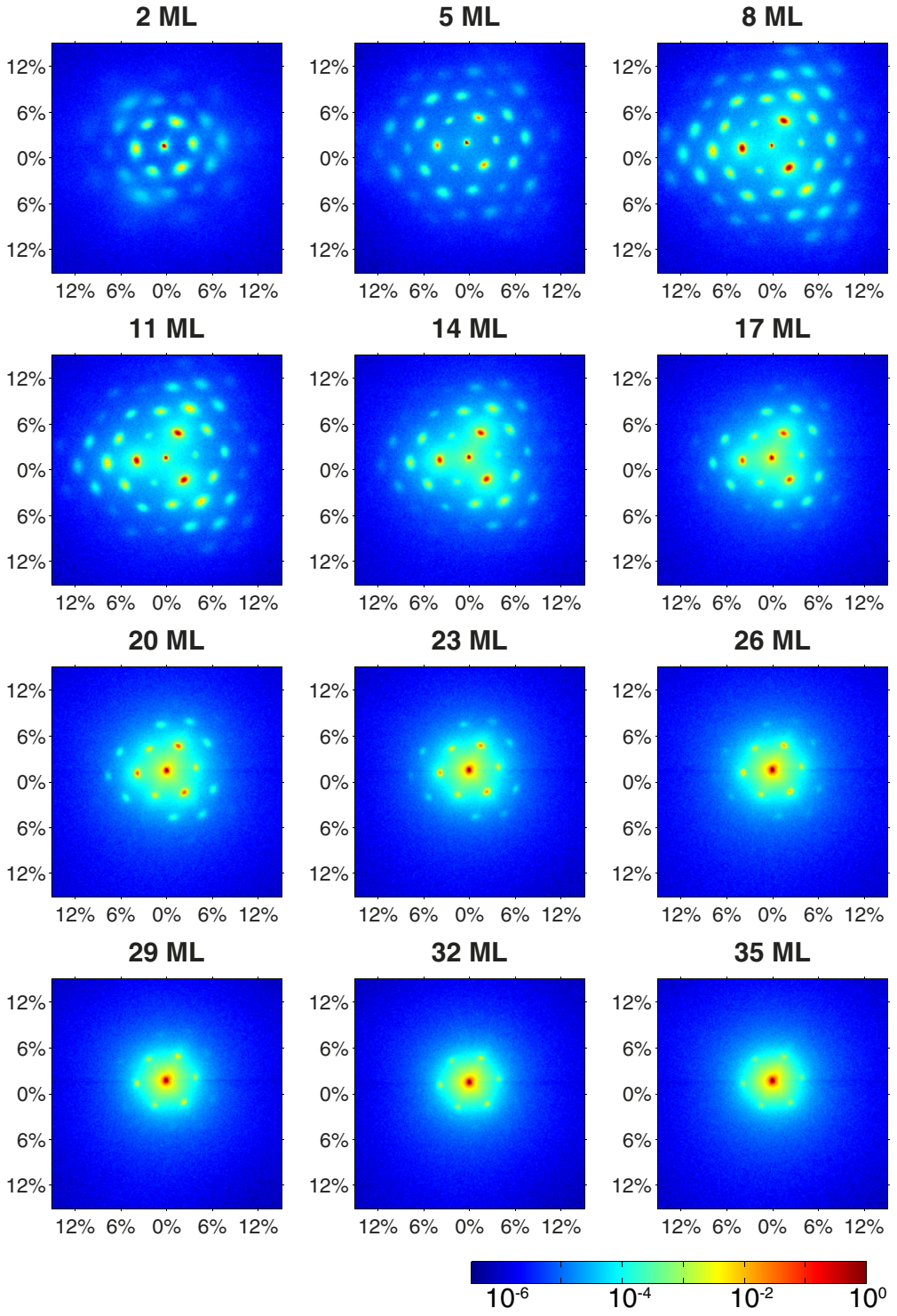

FIG. 7. (Color online) Series of (00) spot patterns after deposition of silver films, with different thicknesses as indicated, on Pt(111) at 800 K. The intensity of the spots is normalized with respect to the height of the specular spot and is presented on a logarithmic scale. The energy of the electrons is 334 eV. The x and y axes of the diffraction patterns are the percentage of BZ calibrated to a clean Pt(111).

This reflects the increased order of the distance between the dislocation lines with increasing film thickness. Note that again the major effect occurs in the first few ML. This reflects the increasing repulsive interactions between the strain fields of the dislocations. Note that an increased reduction of the FWHM sets in above 25 ML. We attribute this to increased ordering in the transition from threefold to sixfold symmetry, as discussed above.

As mentioned further above, we believe that partial intermixing near the interface plays a role in the distance between the dislocations. In agreement with Refs. [11,12] we see that the dislocations separate the fcc and hcp domains. The

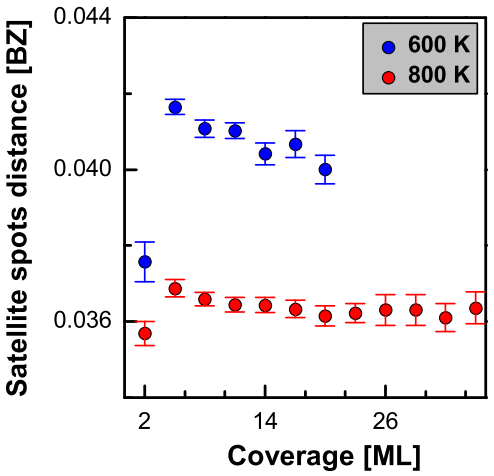

FIG. 8. (Color online) Distance between satellite spots for deposition of silver films at 600 and 800 K as a function of film thickness.

results are partial Shockley dislocations with $(1,1,-2)/6$ type Burgers vectors. The strain fields are inhomogeneous [29], and therefore, one may also expect inhomogeneous local concentrations of Pt in the Ag matrix near the surface. This would result in lateral variations of the nearest-neighbor distances and thus a broadening of the $(\bar{1}0)$ diffraction peak. Note that the width of the specular spot will not be affected. The resulting FWHMs of both peaks as a function of film thickness are shown in Fig. 13(c).

For the 2-ML-thick film the FWHM of the specular beam is determined by the instrumental width, the terrace width distribution of the substrate, and the unknown amplitude of the undulation of the film's surface. The overwhelming broadening at high film thicknesses is due to multilayer growth, characteristic of Ag(111) homoepitaxy [30,31]. The effect is about 10% smaller for the $(\bar{1}0)$ peak due to the finite in-plane wave vector change and thus the smaller change of the perpendicular wave vector compared to that of the (00) peak. This explains why the width of the $(\bar{1}0)$ peak

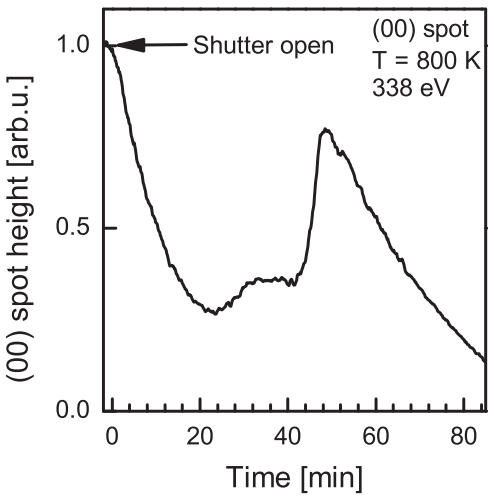

FIG. 9. The normalized height of the (00) spot during deposition of silver at 800 K. The data were taken with 338-eV electrons.

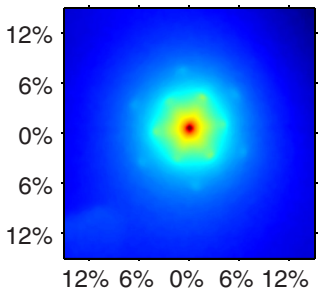

FIG. 10. (Color online) The (00) spot pattern after deposition of 14 ML of Ag on Pt(111) at 600 K, followed by prolonged annealing at 800 K. The energy of the electrons is 334 eV. The x and y axes of the diffraction patterns are the percentage of BZ calibrated to clean Pt(111).

eventually dives underneath that of the specular beam. The specular beam is not affected by uncertainties Δa in the nearest-neighbor distances a due to intermixing of Pt and Ag. The first-order beam is subject to the same broadening factors, and also variation of the nearest-neighbor distances Δa contributes to its width. Its higher initial FWHM is attributed to finite Δa values due to intermixing near the interface. We

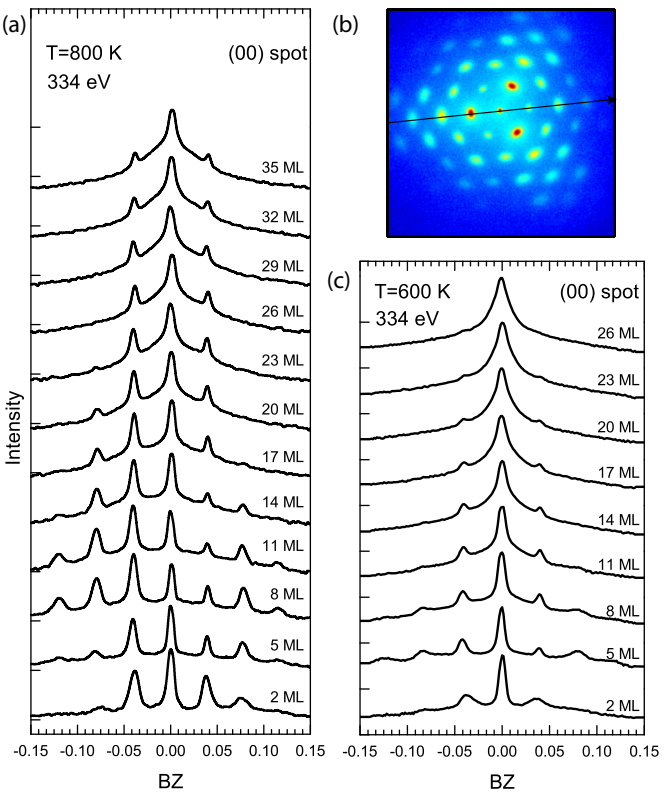

FIG. 11. (Color online) (a) Set of profiles of the (00) spot after deposition of various amounts of silver on Pt(111) at 800 K. (b) Diffraction pattern of the (00) spot after deposition of 8 ML of silver at 800 K; the arrow indicates the direction of the profiles. (c) Set of profiles of the (00) spot after deposition of various amounts of silver on Pt(111) at 600 K. The intensities are plotted on a logarithmic scale, and the data for the various thicknesses have been shifted by an order of magnitude for clarity.

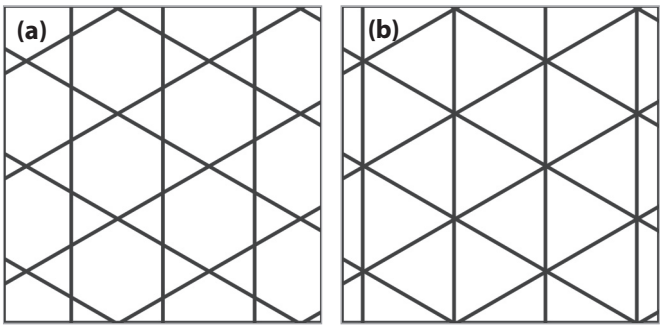

FIG. 12. (a) The arrangement of dislocation lines which forms a network with threefold symmetry. (b) For thicker films the network shows sixfold symmetry due to crossing of the domain walls in one point.

estimate the $\Delta a/a$ value for the 2-ML-thick film at 2%–2.5%. This relatively large number, in view of the overall misfit (3.6%; see Fig. 13), is in line with the heterogeneity of the composition along the interface. This heterogeneity disappears rapidly with increasing film thickness. With increasing film thickness the FWHM of the first-order peak even decreases, which is against the trend caused by multilayer growth. This effect is attributed to a decreasing intermixing and thus smaller Δa in higher layers of the film. We estimate in view of the inelastic mean free path of 334 eV that the intermixing is limited to only the first few layers, counted from the interface.

IV. CONCLUSIONS

We have studied the topography, structure, and composition of Ag films grown on Pt(111) at high temperatures by means of high-resolution electron diffraction. We pay attention to relatively thick films up to 35 ML, a range not investigated in any depth so far, and have studied films grown at 600 and 800 K. These specific temperatures cover the temperature window limited by alloy formation and the desorption of multilayer Ag from Pt(111). The obtained diffraction patterns show the development of satellite spots around integer-order spots. These satellite spots reveal a periodic surface height undulation which originates from a buried dislocation network at the Ag/Pt interface. We confirm the formation of a dislocation network situated at the interface which emerges during deposition of the second monolayer. Remarkably, the mean distance between the dislocation lines depends on temperature and does vary from the expected values based on the bulk lattice mismatch. This is attributed to intermixing near the interface, which causes self-organized lattice matching extending over only a few layers. We also noted that the dislocation network is formed at the growth temperature, and extended annealing at a substantially higher temperature does not lead to significant changes. The degree of intermixing varies along the interface, probably depending on the distance from the dislocation lines.

Due to the propagation of surface height undulations through the silver films the satellite spots are visible up to coverages of 26 and 35 ML at 600 and 800 K, respectively. For the 800 K film the satellite patterns initially exhibit

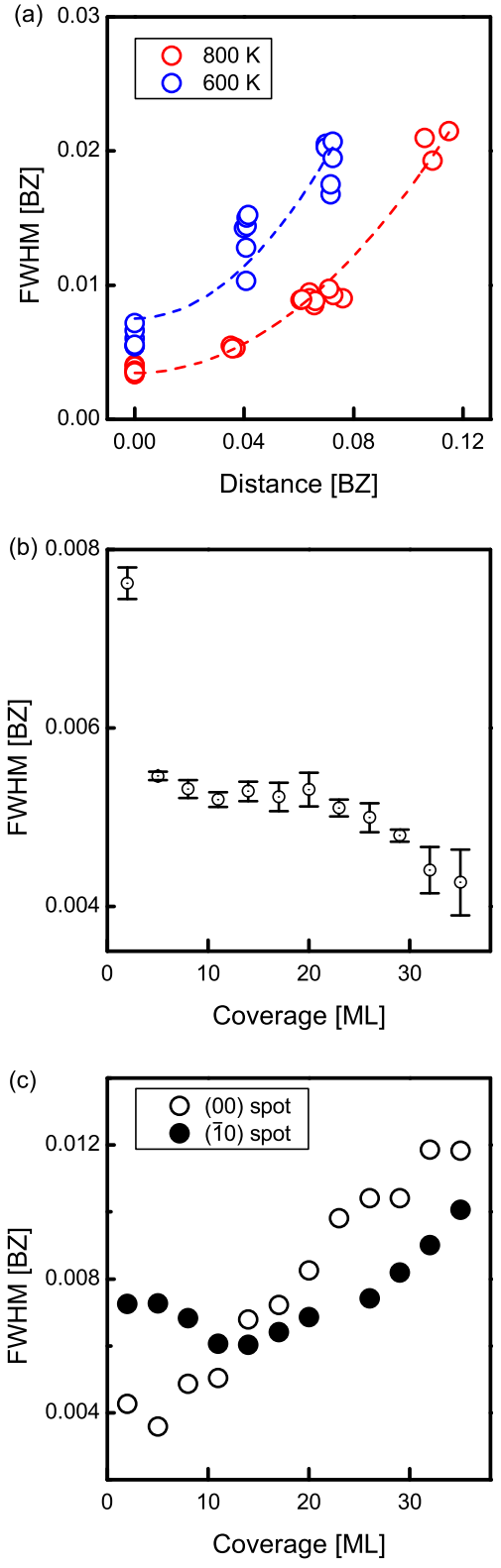

FIG. 13. (Color online) (a) The FWHM of the satellite spots vs their distance from the specular spot for the 8-layer-thick films grown at 800 K and the same for the 8-layer-thick film grown at 600 K. The curves are fits of the data to Eq. (1) with $A = 0.0075$ and 0.0035 and $B = 2.438$ and 1.363 for the 600 and 800 K films, respectively. (b) The width of the first-order satellites near the specular spot vs coverage for films grown at 800 K. (c) The FWHM of the specular beam and that of the $(\bar{1}0)$ beam as a function of the film thickness.

a threefold symmetry which seems to transform into a sixfold symmetry for thicker films. This is attributed to repulsion between the strain fields originating from the buried dislocations.

ACKNOWLEDGMENTS

This work is part of ECHO research program 700.58.026, which is financed by the Chemical Sciences Division of the Netherlands Organisation for Scientific Research (NWO).

[1] C. Günther, J. Vrijmoeth, R. Q. Hwang, and R. J. Behm, Phys. Rev. Lett. **74**, 754 (1995).
[2] J. C. Hamilton and S. M. Foiles, Phys. Rev. Lett. **75**, 882 (1995).
[3] K. Aït-Mansour, P. Ruffieux, W. Xiao, P. Gröning, R. Fasel, and O. Gröning, Phys. Rev. B **74**, 195418 (2006).
[4] K. Aït-Mansour, M. Treier, P. Ruffieux, M. Bieri, R. Jaafar, P. Gröning, R. Fasel, and O. Gröning, J. Phys. Chem. C **113**, 8407 (2009).
[5] H. Brune, M. Giovannini, K. Bromann, and K. Kern, Nature (London) **394**, 451 (1998).
[6] M. Mavrikakis, B. Hammer, and J. K. Nørskov, Phys. Rev. Lett. **81**, 2819 (1998).
[7] B. Diaconescu, G. Nenchev, J. Jones, and K. Pohl, Microsc. Res. Tech. **70**, 547 (2007).
[8] A. F. Becker, G. Rosenfeld, B. Poelsema, and G. Comsa, Phys. Rev. Lett. **70**, 477 (1993).
[9] H. Röder, R. Schuster, H. Brune, and K. Kern, Phys. Rev. Lett. **71**, 2086 (1993).
[10] H. Brune, H. Röder, C. Boragno, and K. Kern, Phys. Rev. B **49**, 2997 (1994).
[11] K. Aït-Mansour, H. Brune, D. Passerone, M. Schmid, W. Xiao, P. Ruffieux, A. Buchsbaum, P. Varga, R. Fasel, and O. Gröning, Phys. Rev. B **86**, 085404 (2012).
[12] A. Bendounan, J. Braun, J. Minár, S. Bornemann, R. Fasel, O. Gröning, Y. Fagot-Revurat, B. Kierren, D. Malterre, F. Sirotti, and H. Ebert, Phys. Rev. B **85**, 245403 (2012).
[13] M. Horn-von Hoegen, F. K. LeGoues, M. Copel, M. C. Reuter, and R. M. Tromp, Phys. Rev. Lett. **67**, 1130 (1991).
[14] P. Zeppenfeld, M. Krzyzowski, C. Romainczyk, R. David, G. Comsa, H. Röder, K. Bromann, H. Brune, and K. Kern, Surf. Sci. **342**, L1131 (1995).
[15] B. Poelsema, L. K. Verheij, and G. Comsa, Phys. Rev. Lett. **53**, 2500 (1984).
[16] H. Brune and K. Kern, in *Growth and Properties of Ultrathin Epitaxial Layers*, edited by D. King and D. Woodruff, Chemical Physics of Solid Surfaces Vol. 8 (Elsevier, Amsterdam, 1997), pp. 149–206.
[17] U. Gradmann and G. Waller, Surf. Sci. **116**, 539 (1982).
[18] M. Horn-von Hoegen, M. Pook, A. Falou, B. Müller, and M. Henzler, Surf. Sci. **284**, 53 (1993).
[19] G. Jnawali, H. Hattab, C. Bobisch, A. Bernhart, E. Zubkov, R. Möller, and M. Horn-von Hoegen, Surf. Sci. **603**, 2057 (2009).
[20] M. Horn-von Hoegen, T. Schmidt, G. Meyer, D. Winau, and K. H. Rieder, Phys. Rev. B **52**, 10764 (1995).
[21] M. Wasniowska, N. Janke-Gilman, W. Wulfhekel, M. Przybylski, and J. Kirschner, Surf. Sci. **601**, 3073 (2007).
[22] M. Horn-von Hoegen, A. Al-Falou, H. Pietsch, B. Müller, and M. Henzler, Surf. Sci. **298**, 29 (1993).
[23] H. Röder, Ph.D. thesis, École polytechnique fédérale de Lausanne, 1994.
[24] R. Schuster, H. Roder, K. Bromann, H. Brune, and K. Kern, Phys. Rev. B **54**, 13476 (1996).
[25] P. Davies, M. Quinlan, and G. Somorjai, Surf. Sci. **121**, 290 (1982).
[26] M. T. Paffett, C. T. Campbell, and T. N. Taylor, Langmuir **1**, 741 (1985).
[27] T. Härtel, U. Strüber, and J. Küppers, Thin Solid Films **229**, 163 (1993).
[28] M. Horn-von Hoegen and M. Henzler, Phys. Status Solidi A **146**, 337 (1994).
[29] J. V. Barth, H. Brune, G. Ertl, and R. J. Behm, Phys. Rev. B **42**, 9307 (1990).
[30] H. A. van der Vegt, H. M. van Pinxteren, M. Lohmeier, E. Vlieg, and J. M. C. Thornton, Phys. Rev. Lett. **68**, 3335 (1992).
[31] G. Rosenfeld, R. Servaty, C. Teichert, B. Poelsema, and G. Comsa, Phys. Rev. Lett. **71**, 895 (1993).